

Supplementary Information

2D Network Overtakes 3D for Photocatalytic Hydrogen Evolution

Aliyu Aremu Ahmad,^a Turkan Gamze Ulusoy Ghobadi,^b Ekmel Ozbay,^{bcd} and

Ferdi Karadas^{*ae}

^a Department of Chemistry, Faculty of Science, Bilkent University 06800 Ankara, Turkey

^b NANOTAM–Nanotechnology Research Center, Bilkent University, 06800 Ankara, Turkey

^c Department of Electrical and Electronics Engineering, Bilkent University, 06800 Ankara, Turkey

^d Department of Physics, Faculty of Science, Bilkent University 06800 Ankara, Turkey

^e UNAM–National Nanotechnology Research Center, Bilkent University, 06800 Ankara, Turkey

*Email: karadas@fen.bilkent.edu.tr (F.K.)

Table of Contents

Experimental section	S3
Supporting Tables	S7
Supporting Figures	S9
References	S22

EXPERIMENTAL SECTION

Chemicals and Reagents. Cobalt(II) nitrate hexahydrate $\text{Co}(\text{NO}_3)_2 \cdot 6\text{H}_2\text{O}$ (Carlo-Erba, $\geq 95\%$), Zinc(II) nitrate hexahydrate $\text{Zn}(\text{NO}_3)_2 \cdot 6\text{H}_2\text{O}$ (Sigma-Aldrich, $\geq 98\%$), Potassium hexacyanoferrate(III) $\text{K}_3\text{Fe}(\text{CN})_6$ (Sigma-Aldrich, $\geq 99\%$), Potassium hexacyanocobaltate(III) $\text{K}_3\text{Co}(\text{CN})_6$ (Sigma-Aldrich, $\geq 97\%$), Potassium tetracyanonickelate(II) hydrate $\text{K}_2\text{Ni}(\text{CN})_4 \cdot x\text{H}_2\text{O}$ (Sigma-Aldrich, $\geq 98\%$), Tris(2,2'-bipyridyl)dichlororuthenium(II) hexahydrate $[\text{Ru}(\text{bpy})_3]\text{Cl}_2 \cdot 6\text{H}_2\text{O}$ (Alfa-Aesar, $\geq 98\%$), Sodium hydroxide NaOH (Sigma-Aldrich, 98–100.5%), and Trifluoroacetic acid CF_3COOH (Merck, $\geq 99\%$) were purchased and used without any further purifications. All the solutions were prepared with Milli Q deionized water (resistivity: 18 $\text{M}\Omega \cdot \text{cm}$).

PBA Catalysts Synthesis.

$\text{Co}[\text{Ni}(\text{CN})_4] \cdot 2.3\text{H}_2\text{O}$, [Co–Ni]. A 50 mL aqueous solution of 0.5 mmol of $\text{Co}(\text{NO}_3)_2 \cdot 6\text{H}_2\text{O}$ was added drop-wisely to an equal volume of an aqueous solution of 0.5 mmol of $\text{K}_2\text{Ni}(\text{CN})_4 \cdot x\text{H}_2\text{O}$ under constant stirring. The resulting solution was stirred vigorously for 2 hours, allowed to stand overnight, centrifuged, washed with de-ionized water, and dried in the oven at 60 °C. A light-magenta precipitate that turned purple upon drying was obtained. Anal. Calcd. (%) for $\text{C}_4\text{H}_{4.6}\text{N}_4\text{O}_{2.3}\text{CoNi}$: C, 18.24; H, 1.75; N, 21.28. Found: C, 18.31; H, 1.69; N, 21.49. EDX Co/Ni atomic ratio: 1/1.

$\text{Zn}[\text{Ni}(\text{CN})_4] \cdot 0.4\text{H}_2\text{O}$, [Zn–Ni]. A 25 mL aqueous solution of 0.5 mmol of $\text{Zn}(\text{NO}_3)_2 \cdot 6\text{H}_2\text{O}$ was added drop-wisely to an equal volume of an aqueous solution of 0.5 mmol of $\text{K}_2\text{Ni}(\text{CN})_4 \cdot x\text{H}_2\text{O}$ under constant stirring. The resulting solution was stirred vigorously for 2 hours and allowed to stand overnight. Then, the obtained white precipitate was centrifuged, washed with de-ionized water, and dried in the oven at 60 °C. Anal. Calcd. (%) for $\text{C}_4\text{H}_{0.8}\text{N}_4\text{O}_{0.4}\text{ZnNi}$: C, 20.40; H, 0.34; N, 23.80. Found: C, 20.24; H, 0.34; N, 23.52. EDX Zn/Ni atomic ratio: 1/1.

$\text{K}_{0.1}\text{Co}_{2.9}[\text{Fe}(\text{CN})_6]_2 \cdot 12\text{H}_2\text{O}$, [Co–Fe]. A 50 mL aqueous solution of 0.75 mmol of $\text{Co}(\text{NO}_3)_2 \cdot 6\text{H}_2\text{O}$ and an equal volume of an aqueous solution of 0.5 mmol of $\text{K}_3\text{Fe}(\text{CN})_6$ under were added simultaneously at a drop-wise rate to 100 mL of de-ionized water under constant stirring at room temp. After complete addition, the resulting solution was stirred vigorously for an additional 1 hour and allowed to stand overnight. Then, the obtained brown

precipitate was centrifuged, washed with de-ionized water, and dried in the oven at 60 °C. Anal. Calcd. (%) for $C_{12}H_{24}N_{12}O_{12}K_{0.1}Co_{2.9}Fe_2$: C, 17.69; H, 2.94; N, 20.61. Found: C, 17.19; H, 2.84; N, 19.52. EDX Co/Fe atomic ratio: 3/2.

$K_{0.1}Co_{2.9}[Co_2(CN)_6]_2 \cdot 14.5H_2O$, [Co–Co]. A 50 mL aqueous solution of 0.75 mmol of $Co(NO_3)_2 \cdot 6H_2O$ was added drop-wisely to an equal volume of an aqueous solution of 0.5 mmol of $K_3Co(CN)_6$ under constant stirring. The resulting solution was stirred vigorously for 2 hours and allowed to stand overnight. Then, the obtained pink precipitate was centrifuged, washed with de-ionized water, and dried in the oven at 60 °C. Anal. Calcd. (%) for $C_{12}H_{29}N_{12}O_{14.5}K_{0.1}Co_{4.9}$: C, 16.63; H, 3.35; N, 19.40. Found: C, 16.82; H, 3.03; N, 19.49.

Physical Measurements. The surface morphology of the catalyst was revealed by transmission electron microscope (TEM, FEI Tecnai G2 F20 X-TWIN) and scanning electron microscope (SEM, FEI QUANTA 200 FEG ESEM). The TEM samples were prepared by dropping 3 μ L of the sample solution (2mg of sample dispensed into 1 mL methanol/water (1:1) mixture) onto the copper grid (carbon film, 400 mesh). The SEM instrument is equipped with an Ametek EDAX Energy Dispersive X-ray (EDX) system for elemental composition analysis. The powder X-ray diffraction (PXRD) patterns were obtained using a PANalytical X'pert PRO X-ray diffractometer using Cu $K\alpha$ radiation (1.5406 Å). Infrared (IR) spectra were recorded on Bruker Alpha Platinum–ATR Spectrometer within the wavenumber range of 400 – 4000 cm^{-1} for 64 scans. X-ray photoelectron spectroscopy (XPS) analysis was performed on Thermo Fisher Scientific K–Alpha X-ray photoelectron spectrometer, using Al $K\alpha$ micro-focused monochromator as the X-ray source and equipped with a flood gun for charge neutralization. All peaks were shifted with reference to C 1s peak position (284.8 eV). Diffuse reflectance UV–Vis absorption spectra were obtained on an Agilent Cary 5000 UV–Vis-NIR spectrophotometer equipped with a diffuse reflectance accessory. Thermogravimetric analysis (TGA) was carried out on a Q500 thermogravimetric analyzer within the temperature range of 28 °C to 650 °C at 5 °C/min under a nitrogen atmosphere. CHN elemental analysis was obtained on Thermo Scientific FLASH 2000 Series CHNS/O elemental analyzer using BBOT as standard and V_2O_5 as a catalyst.

Photocatalytic HER experiment. Photocatalytic experiments were performed in a Pyrex flask sealed with a septum. 1-10 mg catalyst and 1 mM ruthenium photosensitizer ($[Ru(bpy)_3]Cl_2$) were dispersed into a 10 mL aqueous solution of 0.1 M ascorbic acid (pH 5). The pH of the

ascorbic acid solution was adjusted using a 3 M NaOH solution. The Pyrex flask was covered with an aluminum foil before adding the ruthenium complex to prevent an early light-induced reaction. Prior to light irradiation, the mixture was purged with N₂ gas thoroughly for 25 – 30 mins. The photocatalytic experiment was carried out for 3-hours, and the amount of hydrogen gas evolved was determined by injecting 100 μL of the headspace gas at 1-hour interval into a gas chromatograph (Agilent 7820 A, a gas chromatograph equipped with a molecular sieve and a thermal conductivity detector (TCD), using argon as the carrier gas). The experiment was carried out at least twice for each catalyst to obtain a reproducible result. The standard error (σ_M) of the measurements is evaluated from the ratio of the population standard deviation (σ) of the sampling data to the square root of the number of sampling (N), as shown in the equation below.

$$\sigma_M = \frac{\sigma}{N}$$

(eq. S1)

Cycle HER experiments. Before starting a new cycle, the solution containing the used catalyst was centrifuged and washed with deionized water. Then, it is suspended in a fresh solution containing ruthenium photosensitizer and ascorbic acid. The solution is purged with N₂ gas thoroughly for 25 – 30 mins, and the experiment is continued for another 3 hours.

Turn over number (TON) Calculation. The TON per mol of [Co–Ni] was calculated by taking all the cobalt sites as active to catalysis, and using the following formula.

$$\text{Turn over number (TON)} = \frac{\text{moles of } H_2 \text{ evolved from photocatalysis}}{\text{moles of cobalt in [Co-Ni]}}$$

(eq. S2)

The amount of H₂ evolved was obtained from the gas chromatograph, and the moles of cobalt in 2 mg amount of [Co–Ni] was calculated using the relations below.

$$\text{mass of Co in [Co-Ni]} = \% \text{ mass of Co in [Co-Ni]} \times 2 \text{ mg}$$

(eq. S3)

$$\text{moles of Co in [Co-Ni]} = \frac{\text{mass of Co in [Co-Ni]}}{\text{molecular weight of Co}}$$

(eq. S4)

Electrochemical Experiments. Electrochemical experiments were carried out on a Gamry Instruments Interface 1000 potentiostat/galvanostat at 25 °C. Using the conventional three-electrode setup, with Pt mesh as the counter electrode, Ag/AgCl (3.5 M KCl) as the reference electrode, and fluorine-doped tin oxide (FTO) coated electrode (~80% transmittance; 2 mm slides with $7 \Omega \cdot \text{sq}^{-1}$ surface resistivity and 1×2 cm size) as the substrate for working electrode. Electrocatalytic HER activity was evaluated by linear sweep voltammetry experiments performed in a potassium phosphate buffer (KPi) solution at pH 7 containing 1 M KNO_3 as the supporting electrolyte. Cyclic voltammetry experiments were performed at different scan rates ($25 - 125 \text{ mV} \cdot \text{s}^{-1}$) to obtain the surface concentration (Γ) of active cobalt sites from the electrochemical linear plot of the peak current (I_p) of the $\text{Co}^{3+}/\text{Co}^{2+}$ reduction wave versus the scan rate (v).¹

Working Electrode Preparation. 1×2 cm FTO electrode was used as the working electrode, but only 1×1 cm of the conducting surface was coated with the catalyst. Prior to coating the FTO surface, the electrode was adequately cleaned by sonicating for 10 mins in a basic soapy solution, deionized water, and isopropanol, then annealed at 350 °C in the furnace for 30 mins. The surface of FTO was coated with the catalyst by using a drop-casting method. Briefly, 5 mg of the catalyst was added to a mixture of ethanol (400 μL), de-ionized water (100 μL) and Nafion solution (10 μL ; 5 wt%), and then the solution was sonicated for 30 min to obtain a uniform ink. Finally, 5 μL of the obtained ink was drop-casted on the FTO surface, air-dried and kept in the desiccator until measurement.

SUPPORTING TABLES

Table S1: Cyanide stretching frequencies, $\nu(\text{CN})$, of the precursors and the synthesized compounds.

Compound	$\nu(\text{CN})$ (cm^{-1})	Assignment*
$\text{K}_3\text{Fe}(\text{CN})_6$	2115	$\text{Fe}^{3+}-\text{CN}$
[Co-Fe]	2162	$\text{Fe}^{3+}-\text{CN}-\text{Co}^{2+}$
	2117	$\text{Fe}^{2+}-\text{CN}-\text{Co}^{3+}$
	2098	$\text{Fe}^{2+}-\text{CN}-\text{Co}^{2+}$
[Co-Co]	2172	$\text{Co}^{3+}-\text{CN}-\text{Co}^{2+}$
	2133	$\text{Co}^{2+}-\text{CN}-\text{Co}^{3+}$
$\text{K}_2[\text{Ni}(\text{CN})_4] \cdot x\text{H}_2\text{O}$	2119	$\text{Ni}^{2+}-\text{CN}$
[Co-Ni]	2177	$\text{Ni}^{2+}-\text{CN}-\text{Co}^{2+}$
	2141	$\text{Ni}^{2+}-\text{CN}-\text{Co}^{3+}$
[Zn-Ni]	2189	$\text{Ni}^{2+}-\text{CN}-\text{Zn}^{2+}$

*The assignments are listed in accordance with literature.²⁻⁸

Table S2: The obtained chemical formula of the compounds derived from EDX elemental analysis and thermogravimetric analysis (TGA).

Compound	EDX Atomic %						TGA		Chemical Formula
	M	M'	C	N	O	K	% Water molecule		
[Co-Fe]	2.91	2.01	58.5	28.28	7.43	0.1	26.58	$\text{K}_{0.1}\text{Co}_{2.9}[\text{Fe}(\text{CN})_6]_2 \cdot x 12\text{H}_2\text{O}$	
[Co-Co]	11.46	–	39.53	42.84	4.75	0.63	30.12	$\text{K}_{0.1}\text{Co}_{2.9}[\text{Co}(\text{CN})_6]_2 \cdot x 14.5\text{H}_2\text{O}$	
[Co-Ni]	5.40	5.26	41.41	42.28	5.38	–	15.55	$\text{Co}[\text{Ni}(\text{CN})_4] \cdot x 2.3\text{H}_2\text{O}$	
[Zn-Ni]	9.12	9.08	39.53	35.96	6.06	–	3.03	$\text{Zn}[\text{Ni}(\text{CN})_4] \cdot x 0.4\text{H}_2\text{O}$	

Table S3: CHN elemental analysis of the synthesized compounds.^a

Compound	Chemical Formula	Calculated / Found (CHN)		
		%C	%N	%H
[Co–Fe]	$K_{0.1}Co_{2.9}[Fe(CN)_6]_2 \times 12H_2O$	17.69 / 17.19	20.61 / 19.52	2.94 / 2.84
[Co–Co]	$K_{0.1}Co_{2.9}[Co(CN)_6]_2 \times 14.5H_2O$	16.63 / 16.82	19.40 / 19.49	3.35 / 3.03
[Co–Ni]	$Co[Ni(CN)_4] \times 2.3H_2O$	18.24 / 18.31	21.28 / 21.49	1.75 / 1.69
[Zn–Ni]	$Zn[Ni(CN)_4] \times 0.4H_2O$	20.40 / 20.24	23.80 / 23.52	0.34 / 0.34

^aThe results obtained revealed that the calculated values from the derived chemical formula of the compounds agree well with CHN elemental analysis.

Table S4: Comparisons of the photocatalytic hydrogen evolution activities of various heterogeneous catalyst systems.

Catalyst	PS	Electron donor	Activity ($\mu\text{mol/g/h}$)	Ref
[Co–Ni]	Ru	Ascorbic Acid	30,029	This work
[Co–Fe]	Ru	Ascorbic Acid	216	This work
[Co–Co]	Ru	Ascorbic Acid	617	This work
PBA–TiO ₂ Janus	–	TEOA	198	9
g-C ₃ N ₄ –Fe ₂ N nanocomposite	–	TEOA	88.7	10
Co ₃ O ₄	Eosin Y	TEOA	5,552	11
Co ₃ O ₄	–	Ethanol	2000	12
CoCoPBA/CdS	–	Lactic acid	57,288	13
CoNiS _x -CN	–	TEOA	2366	14
Co ₂ C nanoflakes	CdSe/CdS QDs	TEA	18,000	15
azine-based N _x -COFs	–	TEOA	782	16
CoP-CdS/g-C ₃ N ₄	–	TEOA	23,536	17
MoS ₂ /RGO	[ZnTMPyP]4+	TEOA	2560	18
2D–2D SnS ₂ /TiO ₂	–	methanol	652.4	19

ReS ₂ NWs	–	Na ₂ S–Na ₂ SO ₃	13,023	20
NiS/Zn _x Cd _{1-x} S	–	Na ₂ S–Na ₂ SO ₃	16,780	21
NiP	CQD	EDTA	398	22
Ni _x Cd _y S	–	Na ₂ S–Na ₂ SO ₃	8,450	23
NiO	Eosin Y	TEOA	7,757	11

SUPPORTING FIGURES

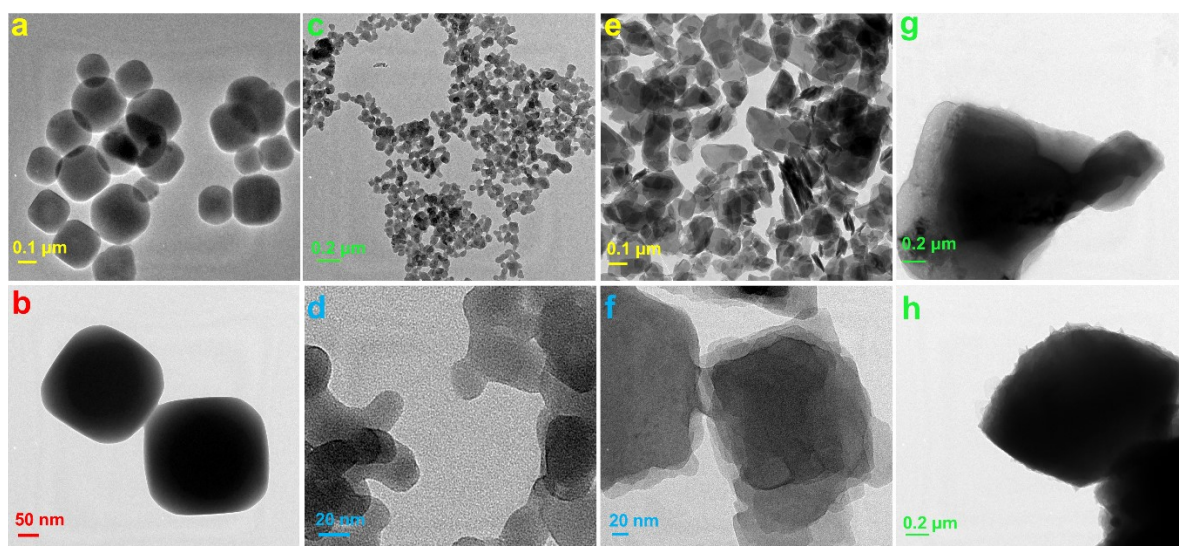


Fig. S1: TEM micrographs of (a,b) [Co–Fe], (c,d) [Co–Co], (e,f) [Co–Ni] and (g,h) [Zn–Ni]. Scale bars: yellow (0.1 μm); red (50 nm); blue (20 nm); green (0.2 μm).

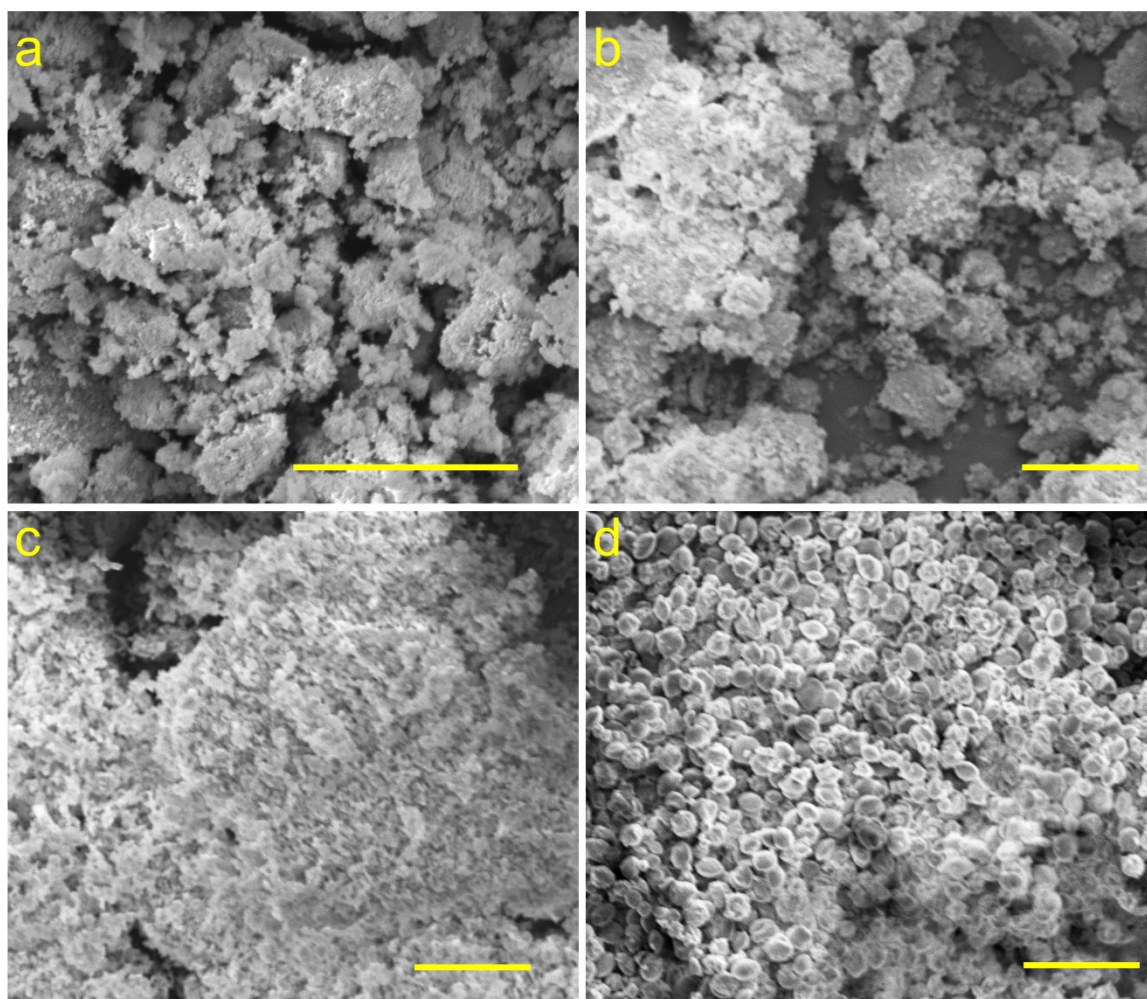


Fig. S2: SEM micrographs of (a) [Co-Fe], (b) [Co-Co], (c) [Co-Ni] and (d) [Zn-Ni]. Scale bars: yellow (10 μm).

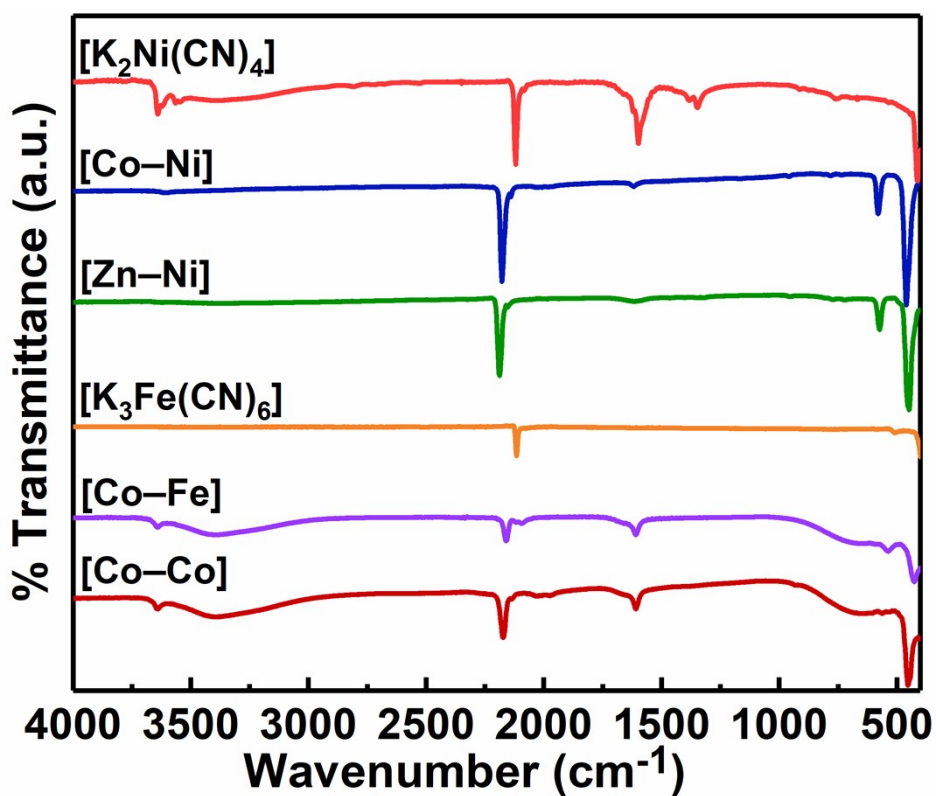


Fig. S3: ATR-FTIR spectra of the precursor and the synthesized PBA compounds ranging from 4000–400 cm⁻¹.

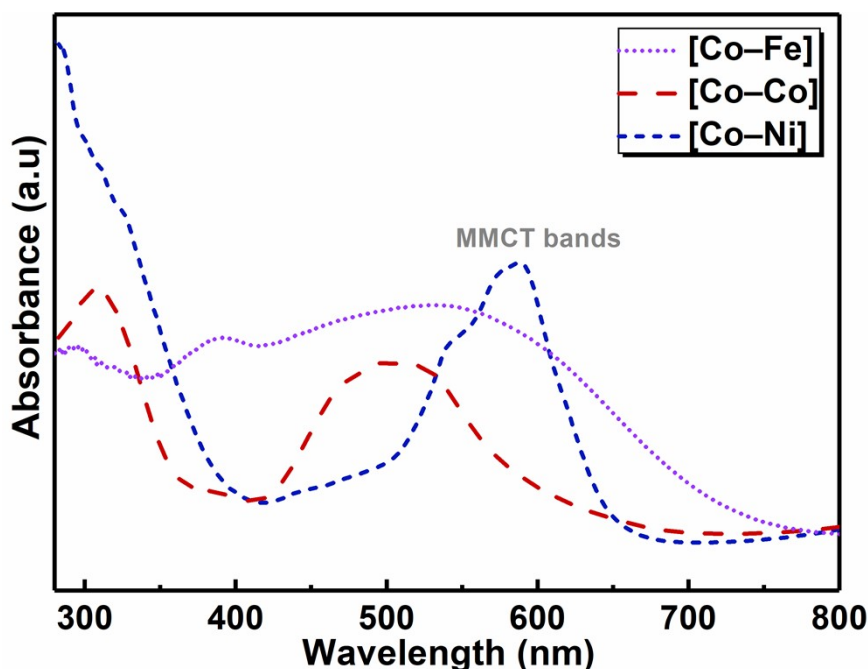


Fig. S4: Diffuse reflectance UV-Vis spectra of [Co-Ni], [Co-Fe] and [Co-Co]. The bands below 400 nm are due to the ligand-to-metal charge transfer (LMCT) or metal-to-ligand charge transfer (MLCT),^{24,25} while the ones above 415 nm are assigned to the metal-to-metal charge transfer (MMCT). The appearance of MMCT bands confirms the formation of a cyanide-bridged network and electronic communication between the two metal sites.²⁶

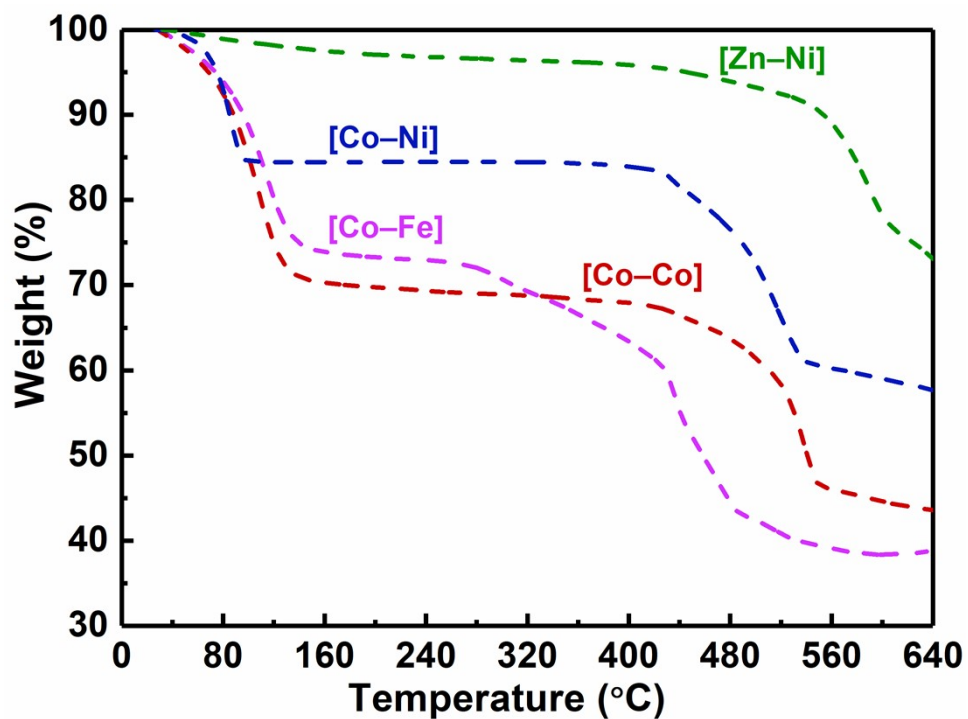


Fig. S5: Thermogravimetric weight loss analysis under N_2 atmosphere in the temperature range of 28 °C to 650 °C at a heating rate of 5 °C/min. The weight loss from 28 °C to 150 °C denotes the removal of coordinated water molecules and those in the interstitial sites/cavities, while the subsequent weight loss pattern above 250 °C indicates the decomposition of the cyanide framework to an oxide.²⁷

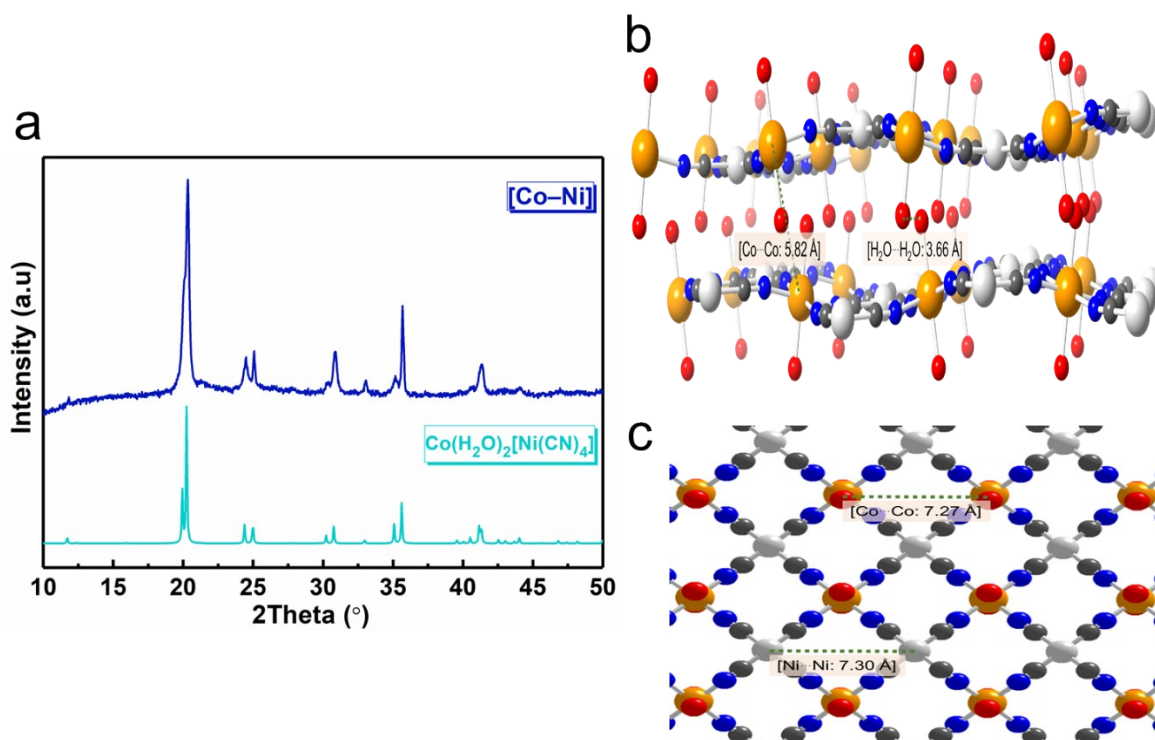


Fig. S6: (a) PXRD pattern of the as-synthesized [Co-Ni] matched perfectly with a reference compound. (b) Side view showing the interlayer distance and (c) top view of the crystal structure of [Co-Ni]. Colour code: Co, orange; Ni, white; C, grey; N, blue; O, red. H atoms of H₂O are omitted for clarity. The reference compound is a standard L₁ phase layered Co(H₂O)₂[Ni(CN)₄]·xH₂O in an *Imma* space group and the crystal structures were created from cif. files deposited at CCDC.⁷

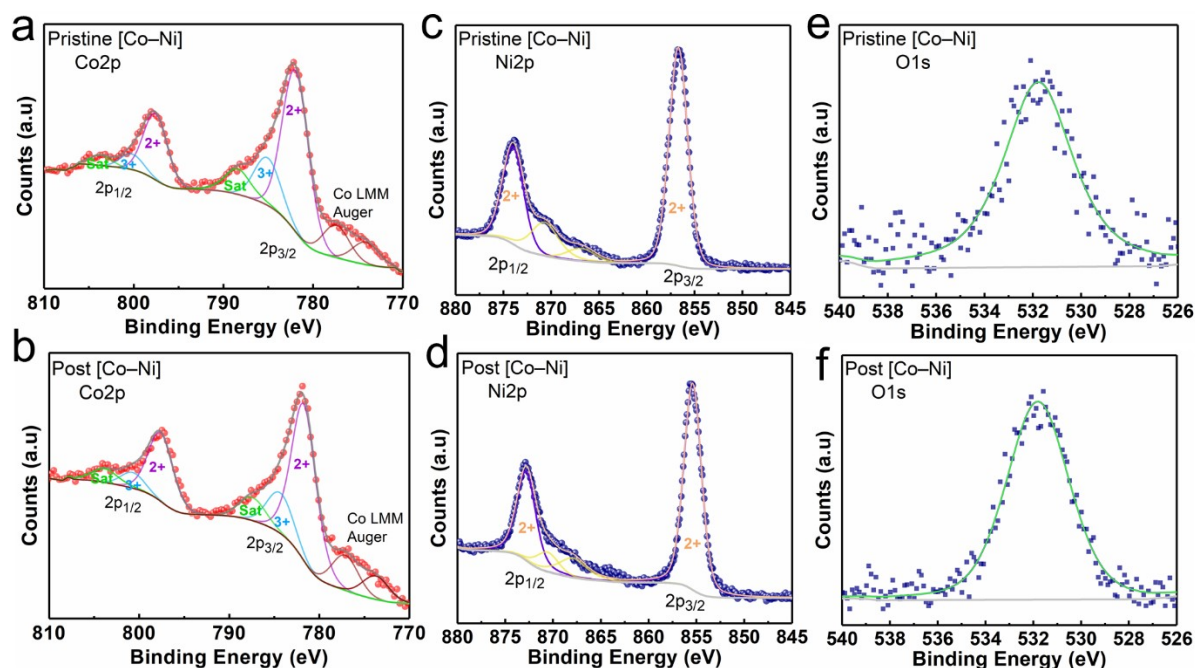


Fig. S7: High-resolution XPS spectra of (a,b) Co2p, (c,d) Ni2p, and (e,f) O1s from the pristine and post-catalytic samples of [Co-Ni]. The obtained Co 2p (~ 770 – 810 eV) and Ni 2p (~ 845 – 880 eV) core level XPS spectra are deconvoluted into $2p_{3/2}$ and $2p_{1/2}$ due to spin-orbit coupling,²⁸ with a Shirley-type background by fitting. The Co 2p peaks are well-fitted into Co^{2+} and Co^{3+} , the presence of Co^{2+} is supported by the presence of shake-up satellite peaks.²⁹ Unfortunately, the strong overlapping of Co and Ni Auger lines with the photoelectron peaks complicates the spectrum. Therefore in Co2p, weak Ni LMM and Co LMM Auger peaks are detected around 778 eV and 775 eV, respectively.^{30–32} The Ni $2p_{3/2}$ and Ni $2p_{1/2}$ signals are fitted into one main peak assigned to Ni^{2+} . The absence of satellite peaks strongly supports that the Ni^{2+} is square planar with diamagnetic nature. Also, a plasmon energy loss related broad peak was observed between the main Ni 2p peaks.³¹

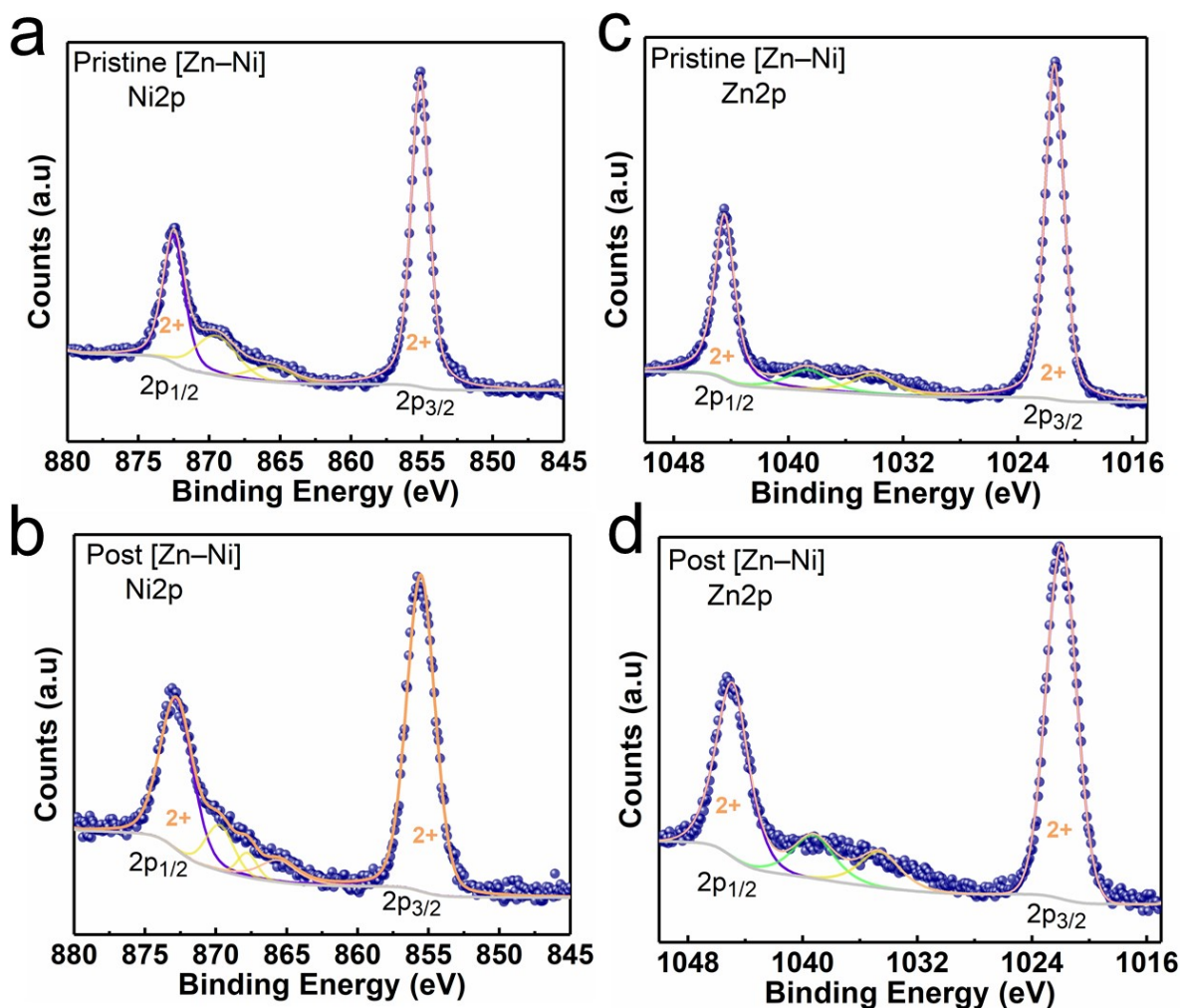


Fig. S8: XPS curve-fitting results of (a,b) Ni 2p, (c,d) Zn 2p spectra from pristine and post [Zn–Ni] samples. The obtained Zn 2p ($\sim 1016 - 1050$ eV) and Ni 2p ($\sim 845 - 880$ eV) core level XPS peaks also splits into $2p_{3/2}$ and $2p_{1/2}$ due to spin-orbit coupling.²⁸ Spin states of both Zn 2p and Ni 2p are fitted into one main peak assigned to $2+$ oxidation state. The absence of satellite peaks strongly supports that the Zn^{2+} has a completely filled d-orbital and Ni^{2+} is square planar and diamagnetic. The existence of multiple small peaks at energies below $2p_{1/2}$ spin correspond to the plasmon energy loss features.³¹

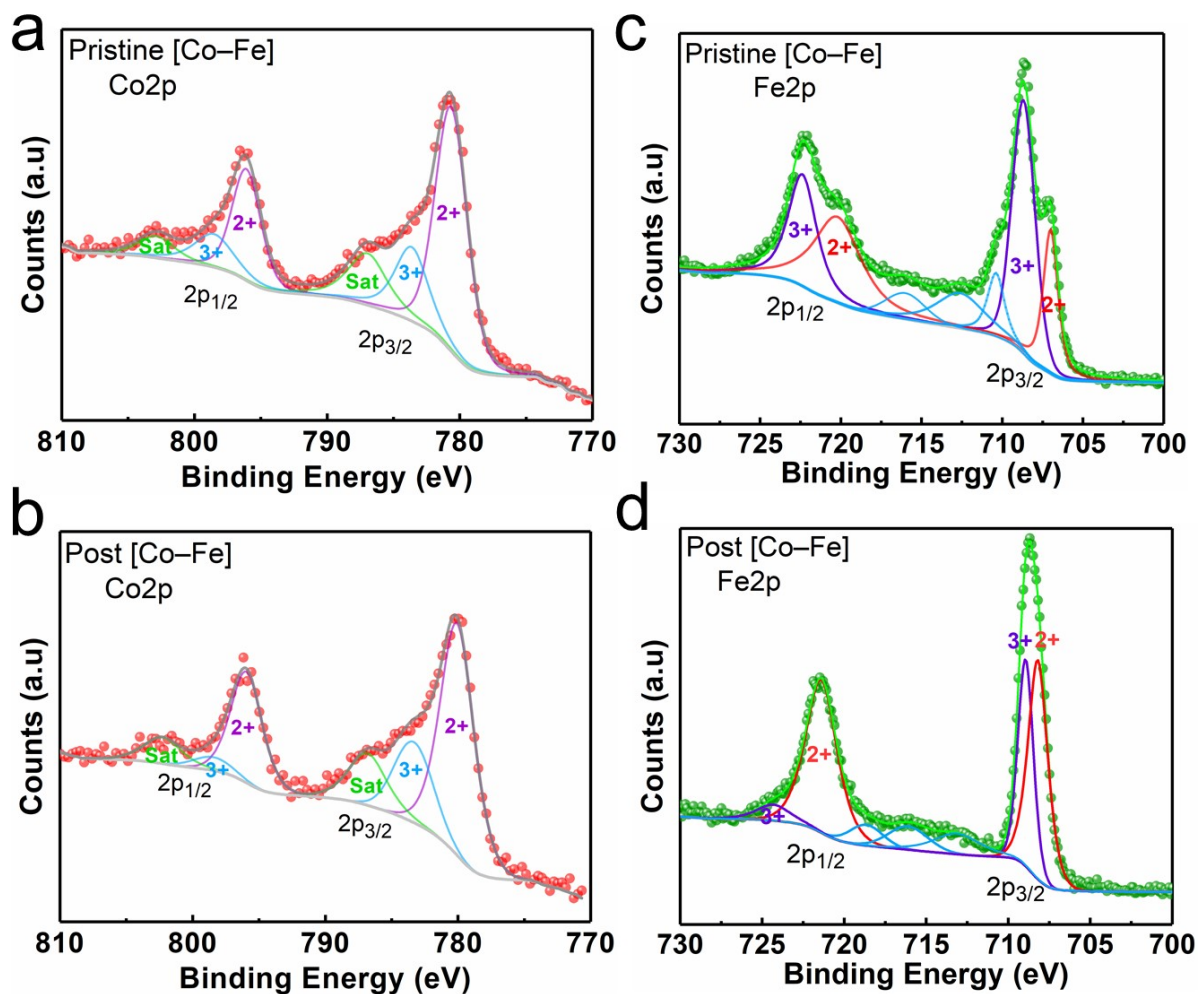


Fig. S9: XPS curve-fitting results of (a,b) Co 2p, (c,d) Fe 2p spectra from pristine and post [Co–Fe] samples. The obtained Co 2p ($\sim 770 - 810$ eV) and Fe 2p ($\sim 700 - 730$ eV) signals splits into $2p_{3/2}$ and $2p_{1/2}$ due to spin-orbit coupling.²⁸ The assignment of the Fe 2p peaks are analyzed into Fe^{2+} and Fe^{3+} , likewise, the Co 2p peak is divided into Co^{2+} and Co^{3+} accordingly.³³ The strong shake-up satellite peaks in Co 2p signals are due to the existence of Co^{2+} .²⁸ The slight peak shift in the post-catalytic samples is attributed to the reduction of Fe^{3+} to Fe^{2+} , which is also reflected in the FTIR spectra.

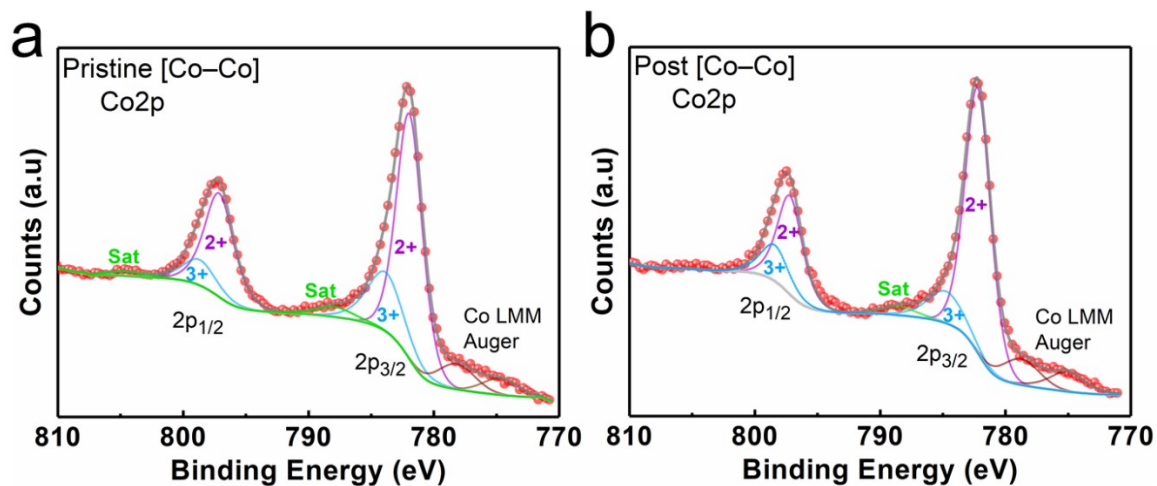


Fig. S10: XPS curve-fitting results of Co 2p peaks spectra from (a) pristine and (b) post [Co–Co] samples. The only transition metal signal obtained is the Co 2p peak ($\sim 770 - 810$ eV), which also splits into $2p_{3/2}$ and $2p_{1/2}$ due to spin-orbit coupling.²⁸ Both the Co $2p_{3/2}$ and Co $2p_{1/2}$ peaks is a combination of Co^{2+} and Co^{3+} based on the spin-orbit splitting values. The multiple peaks located at 770-780 eV range are attributed to the Co LMM Auger peaks.³²

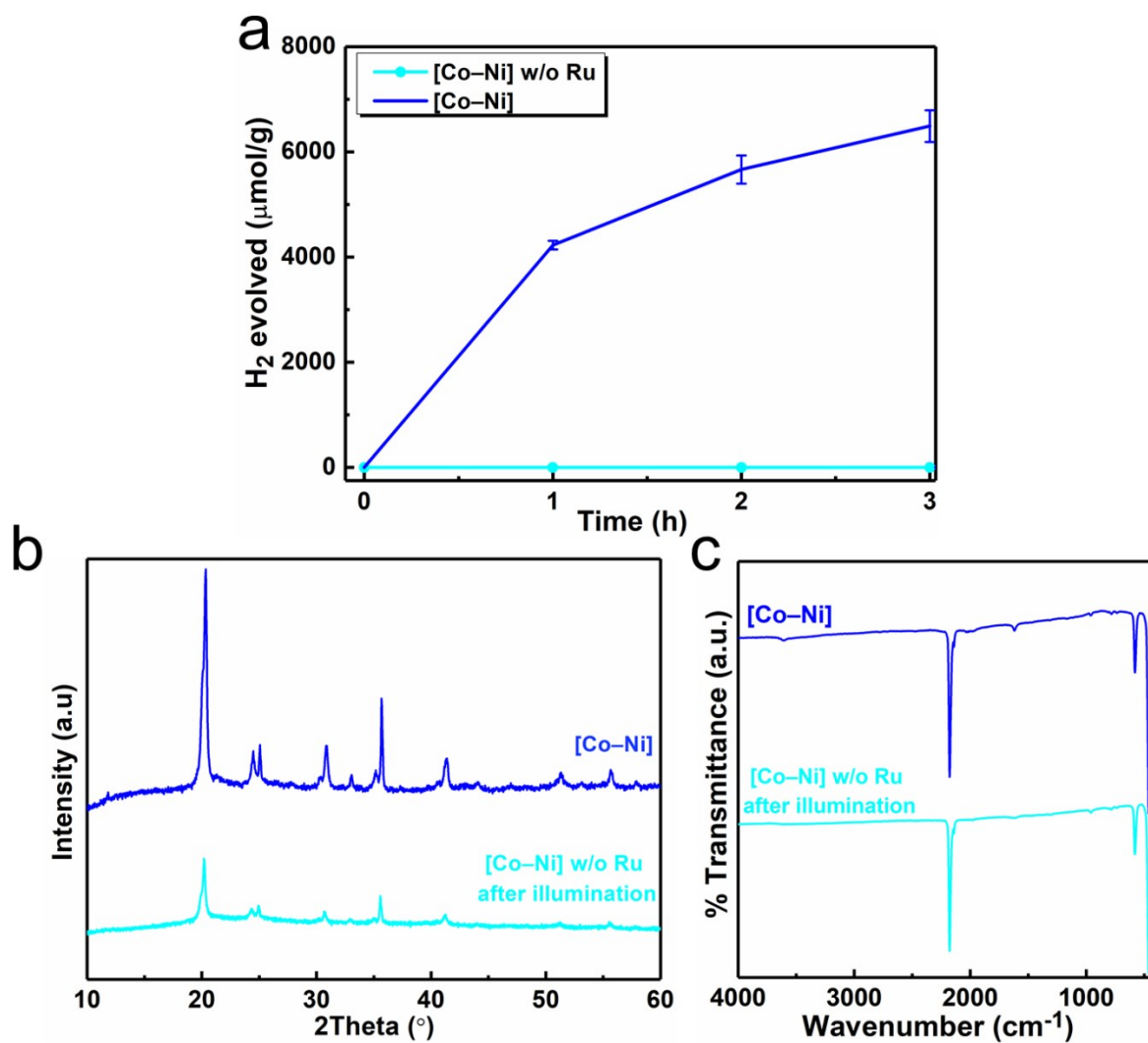


Fig. S11: (a) Photocatalytic HER experiments of [Co-Ni] with and without Ru PS. Conditions: 10 mg Catalyst, 100 mM ascorbic acid, pH 5, 1 mM [Ru(bpy)₃]Cl₂, and 100 mW.cm⁻² white light source. Post-catalytic (b) PXRD and (c) FTIR characterizations of [Co-Ni] without Ru PS after illumination for 3 hours.

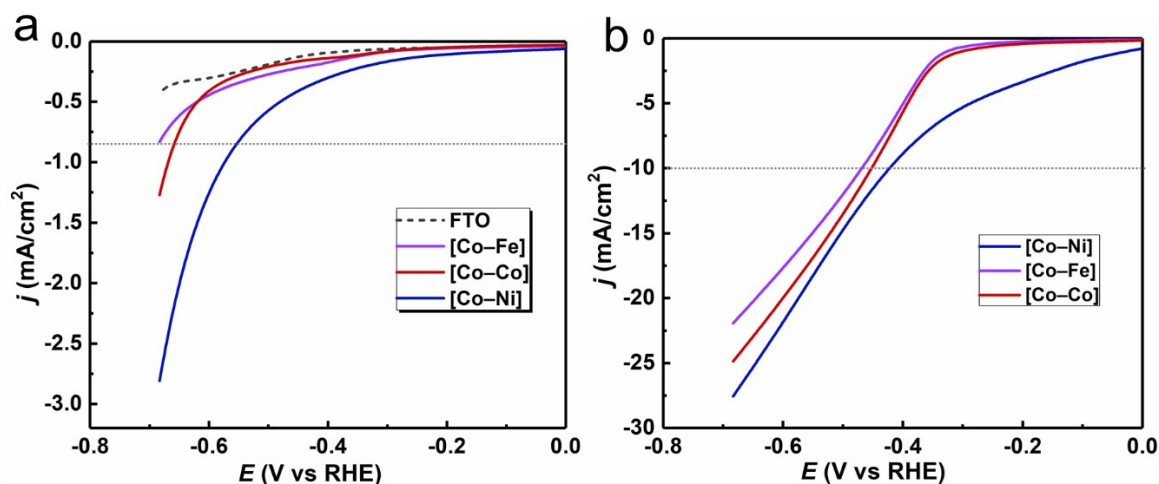


Fig. S12: (a) LSV curves of the compounds on a FTO electrode in 0.1 M KPi electrolyte at pH 7 at a scan rate of 50 mVs^{-1} . (b) LSV curve of the compounds on a FTO electrode upon addition of 10 mM Trifluoroacetic acid (TFA) into the 0.1 M KPi electrolyte. The current enhancement caused by the addition of TFA into the electrolyte solution signifies an increased H_2 evolution.³⁴ All the potentials are converted to V_{RHE} using the Nernst equation³⁵:

$$V_{\text{RHE}} = V_{\text{Ag/AgCl}}(V) + 0.059 \times \text{pH} + V_{\text{Ag/AgCl}}^{\circ}(V)$$

where V_{RHE} is the applied potential versus RHE, $V_{\text{Ag/AgCl}}(V)$ is the applied potential versus Ag/AgCl reference electrode, and $V_{\text{Ag/AgCl}}^{\circ}(V)$ is the standard potential of the reference electrode ($0.197 V_{\text{RHE}}$).

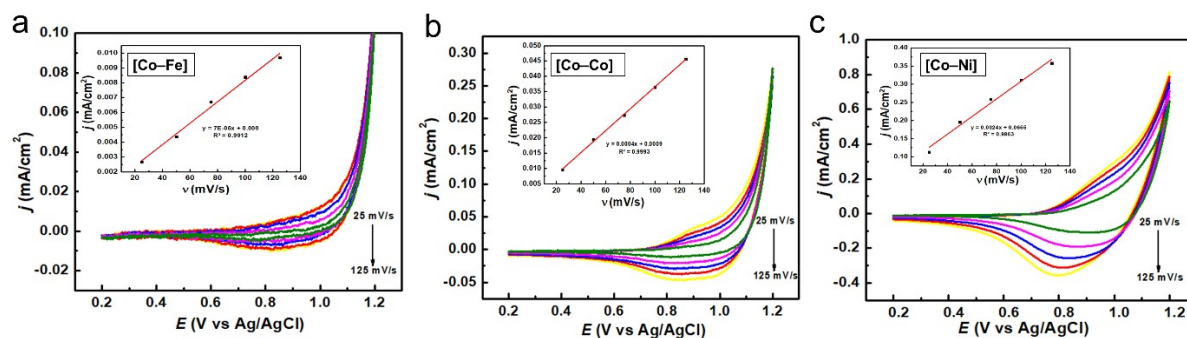


Fig. S13: Cyclic voltammogram of (a) [Co-Fe], (b) [Co-Co] and (c) [Co-Ni] recorded at different scan rate ranging from 25 – $125 \text{ mV}\cdot\text{s}^{-1}$. Inset: linear plot of the peak current (I) of $\text{Co}^{3+}/\text{Co}^{2+}$ reduction wave versus scan rate (v). The CV experiments were performed in a KPi electrolyte solution at pH 7 containing 1 M KNO_3 as the supporting electrolyte. Calculated surface areas are following; $0.07 \text{ nmol}\cdot\text{cm}^{-2}$, $0.43 \text{ nmol}\cdot\text{cm}^{-2}$, $2.55 \text{ nmol}\cdot\text{cm}^{-2}$ for (a) [Co-Fe], (b) [Co-Co] and (c) [Co-Ni], respectively. Although the overall electrocatalytic performances are relatively low due to the reduced conductivity by the Nafion binder used in the electrode preparation and the loose physical interaction between the catalyst and the electrode surface, an activity trend, $[\text{Co-Ni}] > [\text{Co-Co}] > [\text{Co-Fe}]$, is obtained similar to photocatalytic studies.

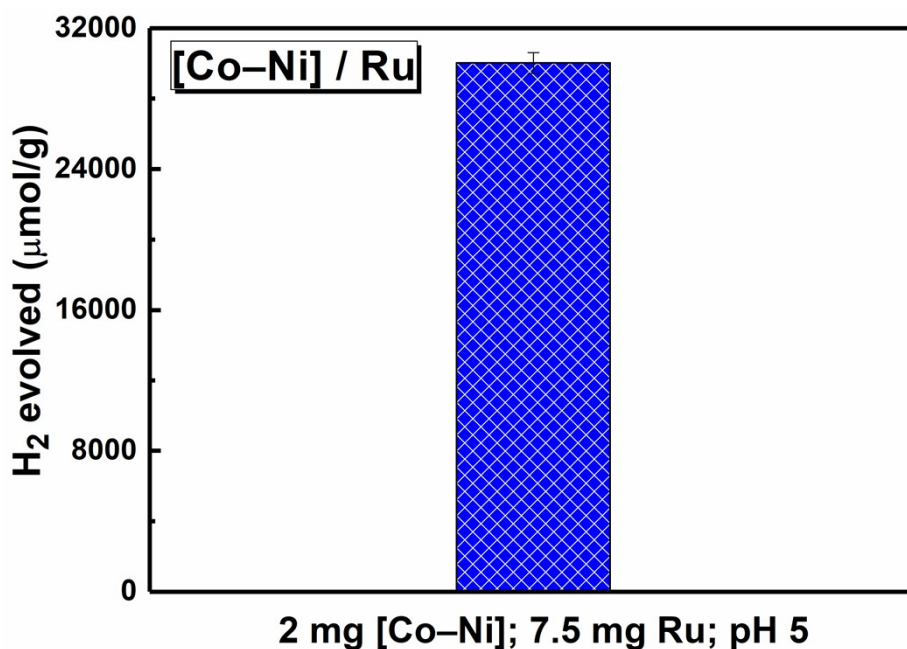


Fig. S14: (a) Optimal photocatalytic HER performance of [Co-Ni]. Conditions: 2 mg Catalyst, 100 mM ascorbic acid, pH 5, 1 mM [Ru(bpy)₃]Cl₂, and 100 mW.cm⁻² white light source.

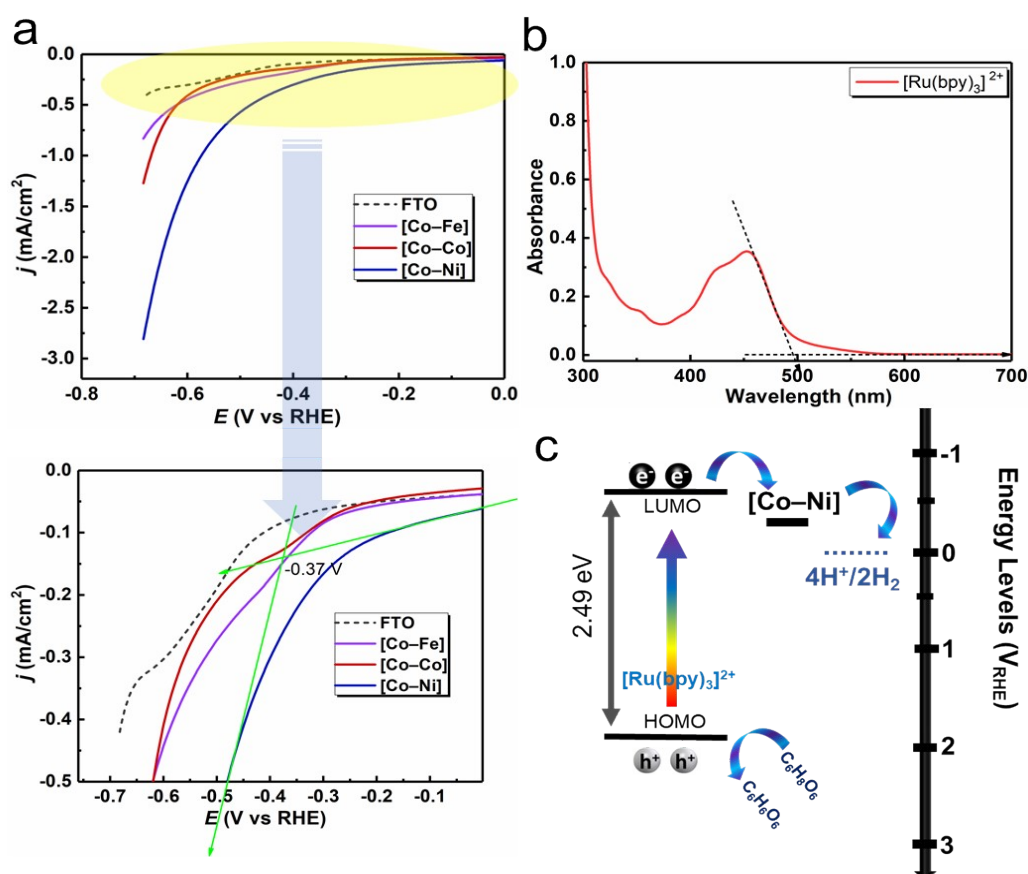


Figure S15. (a) LSV profiles and the zoomed onset potential of [Co-Ni]. (b) UV-Vis spectra of [Ru(bpy)₃]²⁺ in ascorbic acid solution, showing the absorbance tail of around 500 nm. (c) Extracted energy band diagram of [Co-Ni] for the photocatalytic hydrogen reduction process, involving the electron transfer mechanism.

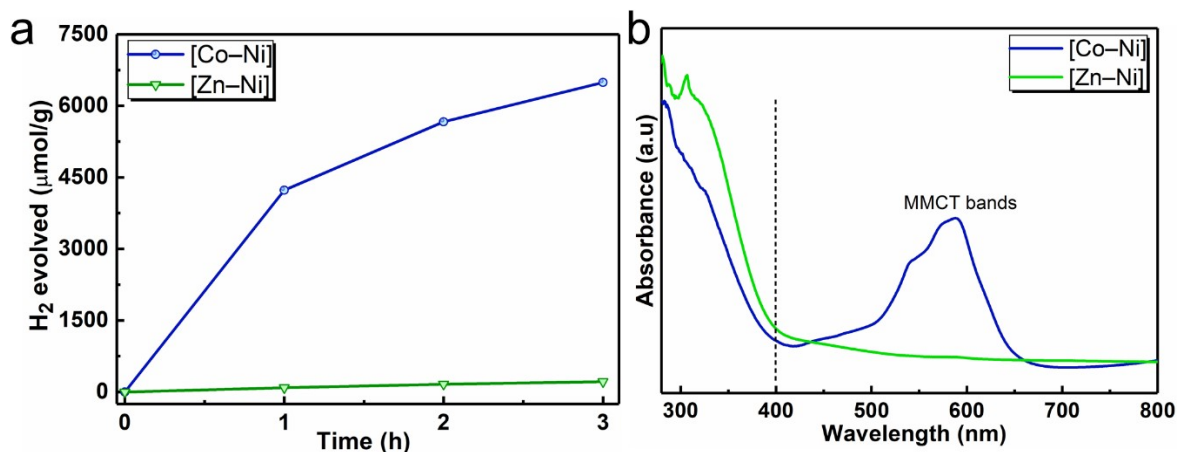


Fig. S16: (a) Comparison of photocatalytic HER performance of [Co-Ni] and [Zn-Ni]. Conditions: 10 mg Catalyst, 100 mM ascorbic acid, pH 5, 1 mM [Ru(bpy)₃]Cl₂, and 100 mW.cm⁻² white light source. (b) Diffuse reflectance UV-Vis spectra of [Co-Ni] and [Zn-Ni]. The absence of MMCT bands in [Zn-Ni] suggest that there is no electron transfer between the Ni and Zn sites.

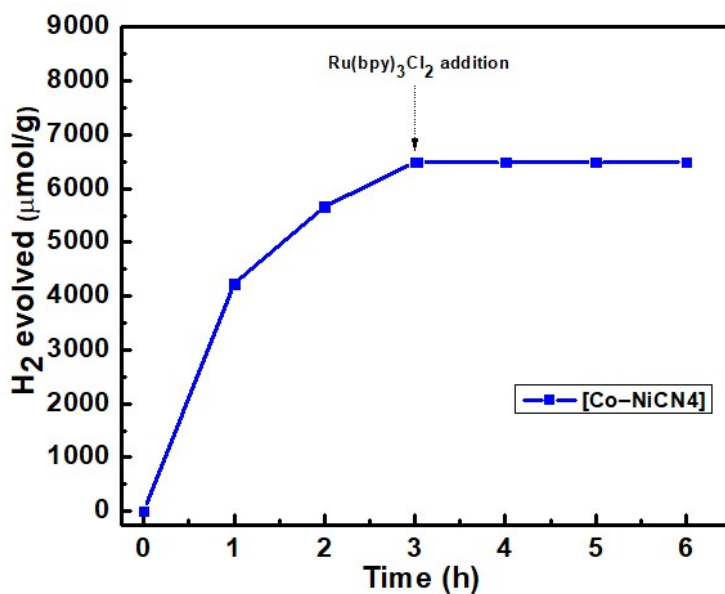


Fig. S17: Photocatalytic HER activity of [Co-Ni] upon addition of fresh 1 mM [Ru(bpy)₃]Cl₂, into the reaction mixture after 3 hours of illumination.

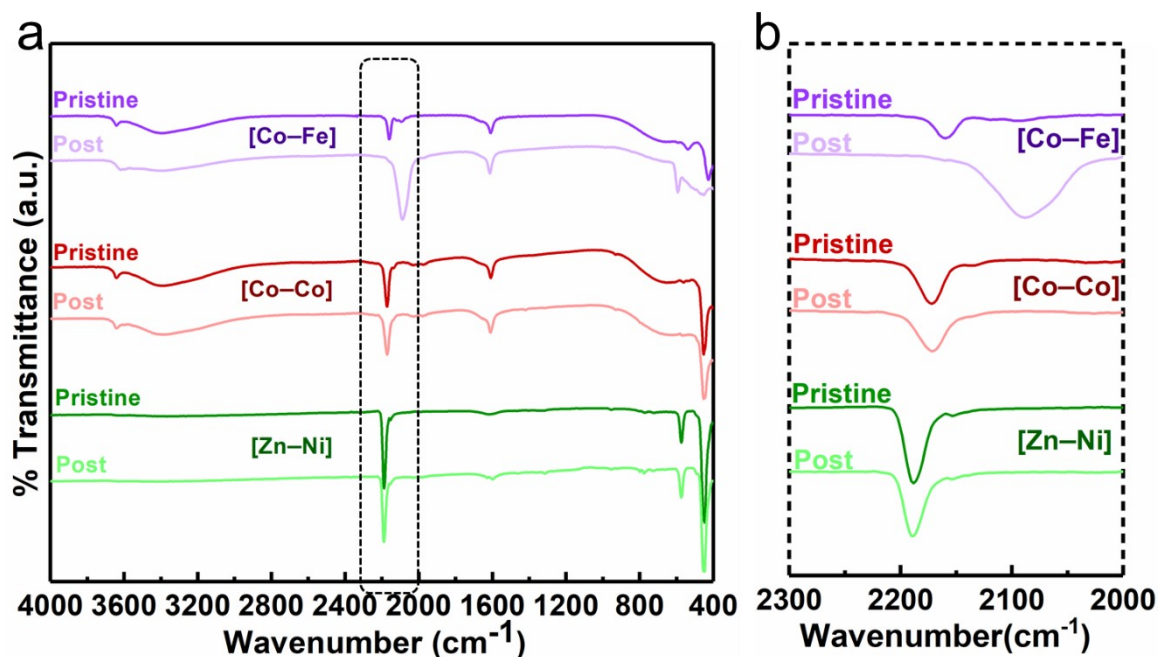


Fig. S18: ATR-FTIR spectra of the pristine and post-catalytic samples of [Co-Fe], [Co-Co], and [Zn-Ni] showing (a) the full spectrum ranging from 4000 to 400 cm^{-1} and (b) zoomed cyanide stretching region ranging from 2300 to 2000 cm^{-1} .

REFERENCES

- 1 S. Pintado, S. Goberna-Ferrón, E. C. Escudero-Adán and J. R. Galán-Mascarós, *J. Am. Chem. Soc.*, 2013, **135**, 13270–13273.
- 2 A. Azhar, M. B. Zakaria, J. Kim, J. Na, Y. V. Kaneti, A. Fatehmulla, A. M. Aldhafiri, W. Aslam Farooq, Y. Bando, Y. Yamauchi and J. Lin, *Bull. Chem. Soc. Jpn.*, 2019, **92**, 1263–1267.
- 3 D. F. Shriver and D. B. Brown, *Inorg. Chem.*, 1968, **8**, 42–46.
- 4 E. J. Canto-Aguilar, M. A. Oliver-Tolentino, G. Ramos-Sánchez and I. González, *Electrochim. Acta*, 2021, **371**, 137828.
- 5 O. Sato, Y. Einaga, T. Iyoda, A. Fujishima and K. Hashimoto, *J. Phys. Chem. B*, 1997, **101**, 20–22.
- 6 O. Sato, T. Iyoda, A. Fujishima and K. Hashimoto, *Science (80-.)*, 1996, **272**, 704–705.
- 7 J. Rodríguez-Hernández, A. A. Lemus-Santana, C. N. Vargas and E. Reguera, *Comptes Rendus Chim.*, 2012, **15**, 350–355.
- 8 S. Goberna-Ferrón, W. Y. Hernández, B. Rodríguez-García and J. R. Galán-Mascarós, *ACS Catal.*, 2014, **4**, 1637–1641.

- 9 C. Shi, S. Ye, X. Wang, F. Meng, J. Liu, T. Yang, W. Zhang, J. Wei, N. Ta, G. Q. Lu, M. Hu and J. Liu, *Adv. Sci.*, 2021, **8**, 1–8.
- 10 W. Qi, S. Liu, F. Li, H. Jiang, Z. Cheng, S. Zhao and M. Yang, *Catal. Sci. Technol.*, 2019, **9**, 2571–2577.
- 11 G. Yanalak, A. Aljabour, E. Aslan, F. Ozel and I. H. Patir, *Int. J. Hydrogen Energy*, 2018, **43**, 17185–17194.
- 12 P. A. Mangrulkar, M. M. Joshi, S. N. Tijare, V. Polshettiwar, N. K. Labhsetwar and S. S. Rayalu, *Int. J. Hydrogen Energy*, 2012, **37**, 10462–10466.
- 13 M. Zhang, Y. Chen, J.-N. Chang, C. Jiang, W.-X. Ji, L.-Y. Li, M. Lu, L.-Z. Dong, S.-L. Li, Y.-P. Cai and Y.-Q. Lan, *JACS Au*, 2021, **1**, 212–220.
- 14 L. Jiang, K. Wang, X. Wu, G. Zhang and S. Yin, *ACS Appl. Mater. Interfaces*, 2019, **11**, 26898–26908.
- 15 Q. Guo, F. Liang, X. Y. Gao, Q. C. Gan, X. B. Li, J. Li, Z. S. Lin, C. H. Tung and L. Z. Wu, *ACS Catal.*, 2018, **8**, 5890–5895.
- 16 T. Banerjee, F. Haase, G. Savasci, K. Gottschling, C. Ochsenfeld and B. V. Lotsch, *J. Am. Chem. Soc.*, 2017, **139**, 16228–16234.
- 17 P. Wang, T. Wu, C. Wang, J. Hou, J. Qian and Y. Ao, *ACS Sustain. Chem. Eng.*, 2017, **5**, 7670–7677.
- 18 Y. J. Yuan, D. Chen, J. Zhong, L. X. Yang, J. J. Wang, Z. T. Yu and Z. G. Zou, *J. Phys. Chem. C*, 2017, **121**, 24452–24462.
- 19 L. Sun, Z. Zhao, S. Li, Y. Su, L. Huang, N. Shao, F. Liu, Y. Bu, H. Zhang and Z. Zhang, *ACS Appl. Nano Mater.*, 2019, **2**, 2144–2151.
- 20 Q. Zhang, W. Wang, J. Zhang, X. Zhu, Q. Zhang, Y. Zhang, Z. Ren, S. Song, J. Wang, Z. Ying, R. Wang, X. Qiu, T. Peng and L. Fu, *Adv. Mater.*, 2018, **30**, 1–7.
- 21 X. Zhao, J. Feng, J. Liu, W. Shi, G. Yang, G. C. Wang and P. Cheng, *Angew. Chemie - Int. Ed.*, 2018, **57**, 9790–9794.
- 22 B. C. M. Martindale, G. A. M. Hutton, C. A. Caputo and E. Reisner, *J. Am. Chem. Soc.*, 2015, **137**, 6018–6025.
- 23 X. Cao, L. Zhang, C. Guo, T. Chen, C. Feng, Z. Liu, Y. Qi, W. Wang and J. Wang, *Int. J. Hydrogen Energy*, 2022, **47**, 3752–3761.
- 24 L. M. Baraldo, P. Forlano, A. R. Parise, L. D. Slep and J. A. Olabe, *Coord. Chem. Rev.*, 2001, **219–221**, 881–921.
- 25 Y. Nanba, D. Asakura, M. Okubo, Y. Mizuno, T. Kudo, H. Zhou, K. Amemiya, J. Guo and K. Okada, *J. Phys. Chem. C*, 2012, **116**, 24896–24901.
- 26 L. T. Zhang, X. Q. Zhu, S. M. Hu, Y. X. Zhang, S. D. Su, Y. Y. Yang, X. T. Wu and T. L. Sheng, *Dalt. Trans.*, 2019, **48**, 7809–7816.
- 27 C. Aparicio, L. Machala and Z. Marusak, *J. Therm. Anal. Calorim.*, 2012, **110**, 661–669.
- 28 X. Xu, H. Liang, F. Ming, Z. Qi, Y. Xie and Z. Wang, *ACS Catal.*, 2017, **7**, 6394–

- 6399.
- 29 H. J. Niu, Y. P. Chen, R. M. Sun, A. J. Wang, L. P. Mei, L. Zhang and J. J. Feng, *J. Power Sources*, 2020, **480**, 229107.
 - 30 Kratos Analytics., Overlapping photoelectron lines and Auger features are a common issue in the analysis of complex materials. The standard approach of switching to an achromatic Mg X-ray source may become undesirable due to the introduction of X-ray satellites into the spe, <https://www.azom.com/article.aspx?ArticleID=14092>, (accessed April 13, 2022).
 - 31 A. Cano, I. Monroy, M. Ávila, D. Velasco-Arias, J. Rodríguez-Hernández and E. Reguera, *New J. Chem.*, 2019, **43**, 18384–18393.
 - 32 Thermo Fischer Scientific., Cobalt X-ray photoelectron spectra, cobalt electron Config. other Elem. Inf., <https://www.thermofisher.com/tr/en/home/materials-science/learning-center/periodic-table/transition-metal/cobalt.html>, (accessed April 14, 2022).
 - 33 A. A. Ahmad, T. G. Ulusoy Ghobadi, M. Buyuktemiz, E. Ozbay, Y. Dede and F. Karadas, *Inorg. Chem.*, 2022, **61**, 3931–3941.
 - 34 W. R. Mcnamara, Z. Han, P. J. Alperin, W. W. Brennessel, P. L. Holland and R. Eisenberg, *J. Am. Chem. Soc.*, 2011, **133**, 15368–15371.
 - 35 S. Niu, S. Li, Y. Du, X. Han and P. Xu, *ACS Energy Lett.*, 2020, **5**, 1083–1087.